Target-identification and mechanism-of-action studies of indole terpenoid mimics reveal that proper spindle microtubule assembly is essential for Cdh1-mediated proteolysis of CENP-A

Yan Peng,[1,†] Yumeng Zhang,[1,†] Ruan Fang,[1,2,†] Hao Jiang,[3,†] Gongcai Lan,[1] Yajie Liu,[1] Zhaoyang Nie,[2] Shou-De Zhang,[4] Yuyong Ma,[2] Peng Yang,[2] Fengcan Wang,[1] Hong-Hua Ge,[5] Wei-Dong Zhang,[1,6,*] Cheng Luo,[3,*] Ang Li,[2,*] and Weiwei He[1,*]

[1]Shanghai Key Laboratory of New Drug Design, School of Pharmacy, East China University of Science and Technology, Shanghai 200237, China

[2]State Key Laboratory of Bioorganic and Natural Product Chemistry, Shanghai Institute of Organic Chemistry, Chinese Academy of Sciences, Shanghai 200032, China

[3]Drug Discovery and Design Center, State Key Laboratory of Drug Research, Shanghai Institute of Materia Medica, Chinese Academy of Sciences, Shanghai 201203, China

[4]State Key Laboratory of Plateau Ecology and Agriculture, Qinghai University, Xining 810016, China

[5]Institute of Physical Science and Information Technology, Anhui University, Hefei 230601, China

[6]Department of Phytochemistry, School of Pharmacy, Second Military Medical University, Shanghai 200433, China

[†]These authors contributed equally.

*Correspondence: heweiwei@ecust.edu.cn, ali@sioc.ac.cn, cluo@simm.ac.cn, wdzhangy@hotmail.com

Abstract

Centromere protein A (CENP-A) is a centromere-specific protein that determines kinetochore positioning and the accuracy of chromosome segregation. Despite its recognized importance in maintaining mitotic fidelity, the molecular details of CENP-A regulation in mitosis are still obscure. We performed a structure-activity relationship (SAR) study of the cell cycle-arresting indole terpenoid mimic JP18 and identified two more potent analogues, (+)-6-Br-JP18 and (+)-6-Cl-JP18. Tubulin was identified as a potential protein target of these two halogenated analogues by using the drug affinity responsive target stability (DARTS) based method. X-ray crystallographic analysis determined that (+)-6-Br-JP18 and (+)-6-Cl-JP18 bind to the colchicine-binding site of β-tubulin. We further found that treatment of cancer cells with microtubule-targeting agents (MTAs), including these two compounds, upregulated CENP-A by destabilizing Cdh1, an E3 ubiquitin ligase component. The mechanistic study revealed that Cdh1 mediates proteolysis of CENP-A in mitosis, specifying the role of Cdh1 in maintaining mitotic fidelity.

Keywords: indole terpenoid, MTA, DARTS, CENP-A, E3 ubiquitin ligase.

Introduction

Mitosis is a phase of the cell cycle in which a eukaryotic cell divides into two genetically identical cells that contain approximately equal proportions of cellular components.[1,2] The spindle, a dynamic microtubule-based structure that forms during mitosis, is responsible for chromosome segregation.[3] Thus, microtubule assembly and disassembly are considered key steps in mitosis.[4] Disruption of these processes has been used as an effective strategy to suppress tumor cell proliferation.[5] Of note, many microtubule-targeting agents (MTAs) are natural products (e.g. paclitaxel, vincristine, colchicine, and maytansine) or natural product analogues (e.g. ixabepilone and eribulin).[6] Despite their clinical efficacy, the long-term use of MTAs has been found to induce chemoresistance.[7,8] Although the underlying mechanism remains largely unclear, it has been reported to involve the defects in mitotic fidelity, such as aneuploidy and chromosomal instability (CIN).[9–13]

Centromere protein A (CENP-A) is a histone H3 variant that plays a key role in faithful chromosome segregation.[14,15] The centromere is a constricted region of the chromosome that connects sister chromatids.[16] CENP-A replaces histone H3 of the histone octamer at the centromere, allowing the formation of the centromere-specific nucleosome.[14,15] This nucleosome serves as a platform for the assembly of the kinetochore, which connects the chromosome to spindle microtubules.[17,18] Thus, the accuracy of chromosome segregation depends on the proper deposition of CENP-A at the centromere. Overexpression of CENP-A results in mislocalization of this protein to non-centromere regions and formation of the ectopic kinetochore at the chromosome arms, ultimately leading to segregation defects, aneuploidy, and CIN.[15,19,20] Notably, aberrantly high levels of CENP-A are observed in various human tumors and are significantly associated with malignant progression and poor patient survival.[21–24]

CENP-A stability and centromeric deposition are regulated by ubiquitination, which is conserved across species.[25,26] Recently, Wang et al. discovered that the CUL4−DDB1−DCAF11 E3 ligase complex mediates the Ser68 phosphorylation-dependent poly-ubiquitylation of CENP-A, which leads to its degradation in human cervical cancer HeLa cells.[27] In addition, Niikura et al. reported that the mono-ubiquitylation of CENP-A at Lys124 promoted by the CUL4A-RBX1-COPS8 E3 ligase complex is required for CENP-A deposition at the centromere in HeLa cells.[28] However, it remains unclear how impaired microtubule assembly is linked to defective CENP-A regulation, which is critical for mechanistic understanding of MTA-induced tumor evolution (e.g. emergence of acquired chemoresistance).

Indole terpenoids are a large class of natural products characterized by a hybrid structure consisting of a terpene moiety and an indole moiety.[29,30] They exhibit a wide range of biological activities, among which anticancer activity is of increasing interest.[31,32] For example, the penitrem-type indole diterpenoids were found to suppress the proliferation, migration, and invasion of human breast cancer cells.[33–35] Taking advantage of our expertise in indole terpenoid synthesis,[36–43] we initiated a program to search for anticancer agents from synthetic indole terpenoids and analogues thereof and to elucidate their mechanisms of action. In our previous study, an indole terpenoid mimic named JP18 was found to induce

cell cycle arrest in the G2/M phase and inhibit cancer cell proliferation.[44] Herein, we report the discovery of two halogenated analogues of JP18, (+)-6-Br-JP18 and (+)-6-Cl-JP18, as more potent cell cycle inhibitors through a structure–activity relationship (SAR) study. Label-free target identification based on drug affinity responsive target stability (DARTS) indicated that tubulin is a potential protein target of these compounds, and X-ray crystallographic analysis showed that they bind to the colchicine-binding site of β-tubulin. Further investigation revealed that disruption of spindle microtubule assembly by MTAs, including (+)-6-Br-JP18 and (+)-6-Cl-JP18, downregulates Cdh1, an E3 ligase component that mediates proteolysis of CENP-A in mitosis.

Results

Identification of two potent cell cycle inhibitors by an SAR study of JP18.

Our previous study showed that JP18 (**1**), an indole terpenoid mimic, inhibited cell proliferation and induced cell cycle arrest in the G2/M phase in human lung cancer A549 cells.[44] To understand the SAR of JP18, we constructed a focused library consisting of a series of analogues of **1** (Figure 1A) through a conjugate addition strategy.[37,42,44] These compounds were prepared in racemic form, and their effects on cell cycle progression in HeLa cells were investigated by flow cytometry. As in A549 cells, **1** also induced dose-dependent cell cycle arrest in the G2/M phase in HeLa cells (Figures 1B and S1). The necessity of the carbonyl group was evaluated by testing the cell cycle-arresting activity of compounds **2** and **3** (Figure 1); the loss of potency indicated the critical role of this functionality. The effects of indole substituents were also examined. The N1-alkylated analogue (**4**) proved to be essentially inactive in the concentration range of 1.0 to 10 μM, and the introduction of a bromine atom at C4, C5, and C7 resulted in a significant decrease in potency (see the data for compounds **5**–**7**). To our delight, 6-Br-JP18 (**8**) exhibited considerably stronger activity than **1**. Analogues with various C6 substituents were then tested. 6-Cl-JP18 (**9**) was found to be as potent as **8**, and **10**–**12** also showed enhanced activity over **1**. In contrast, the C6-florinated analogue (**13**) displayed reduced potency, and compounds **14**–**16** containing larger C6 substituents were essentially inactive in the concentration range tested. Notably, compounds **8** and **9** remained effective in the concentration range of 0.10 to 2.0 μM (Figure S2) compared to **1**, which is

consistent with the measured half-maximal inhibitory concentration (IC_{50}) of **8** and **9** (0.96 and 0.80 μM, respectively) compared to that of **1** (12 μM) (Figure S3).

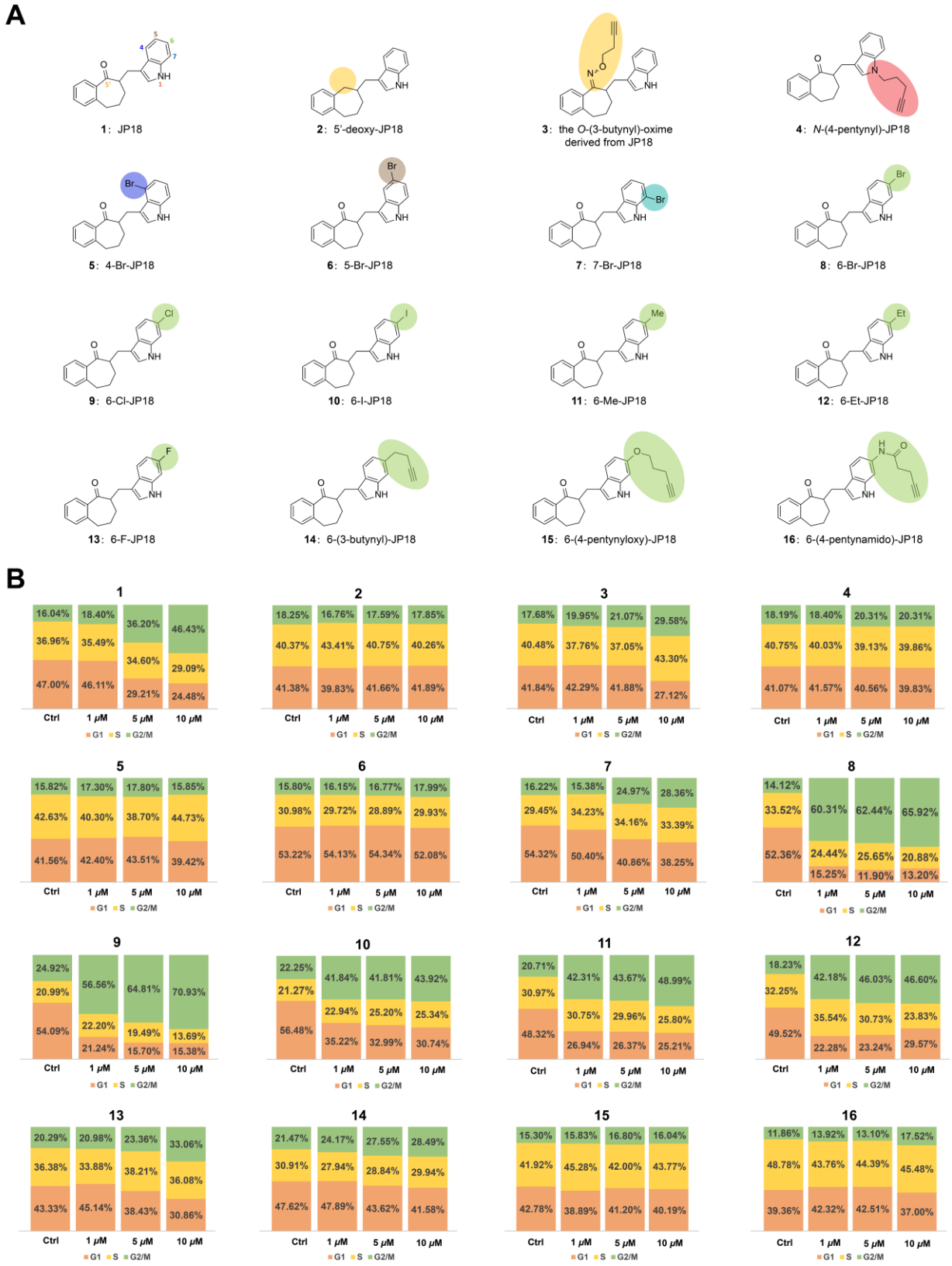

Figure 1. Cell cycle-arresting activity of JP18 and analogues thereof. (A) Chemical structures of JP18 and its fifteen representative analogues. (B) Cell cycle analysis by flow cytometry. HeLa cells were treated with the indicated compounds at the indicated concentrations for 8 h and then stained with propidium iodide (PI). DMSO was used as a control for the compounds. Bar graphs show the percentages of cells in the G2/M (green), S (yellow), and G1 (orange) phases.

We then determined the enantiomeric forms of **8** and **9** responsible for the cell cycle-arresting activity. The racemic samples of **8** and **9** were separated by high-performance liquid chromatography (HPLC) using a chiral stationary phase. Flow cytometry analysis revealed that both (+)-**8** and (+)-**9** induced cell cycle arrest in the G2/M phase in the concentration range of 0.10 to 2.0 μM (Figures 2A and 2B), whereas their enantiomers exhibited much weaker activity (Figure S4). Furthermore, treatment of HeLa cells with both (+)-**8** and (+)-**9** increased cyclin B1 levels and decreased phospho-CDK1 (Tyr15) levels in a dose- and time-dependent manner (Figures 2C and 2D), which confirmed their G2/M phase-arresting activity.[45] Notably, the absolution configuration of (+)-**8** has been elucidated by a combination of asymmetric synthesis and computation, which will be reported elsewhere in due course.

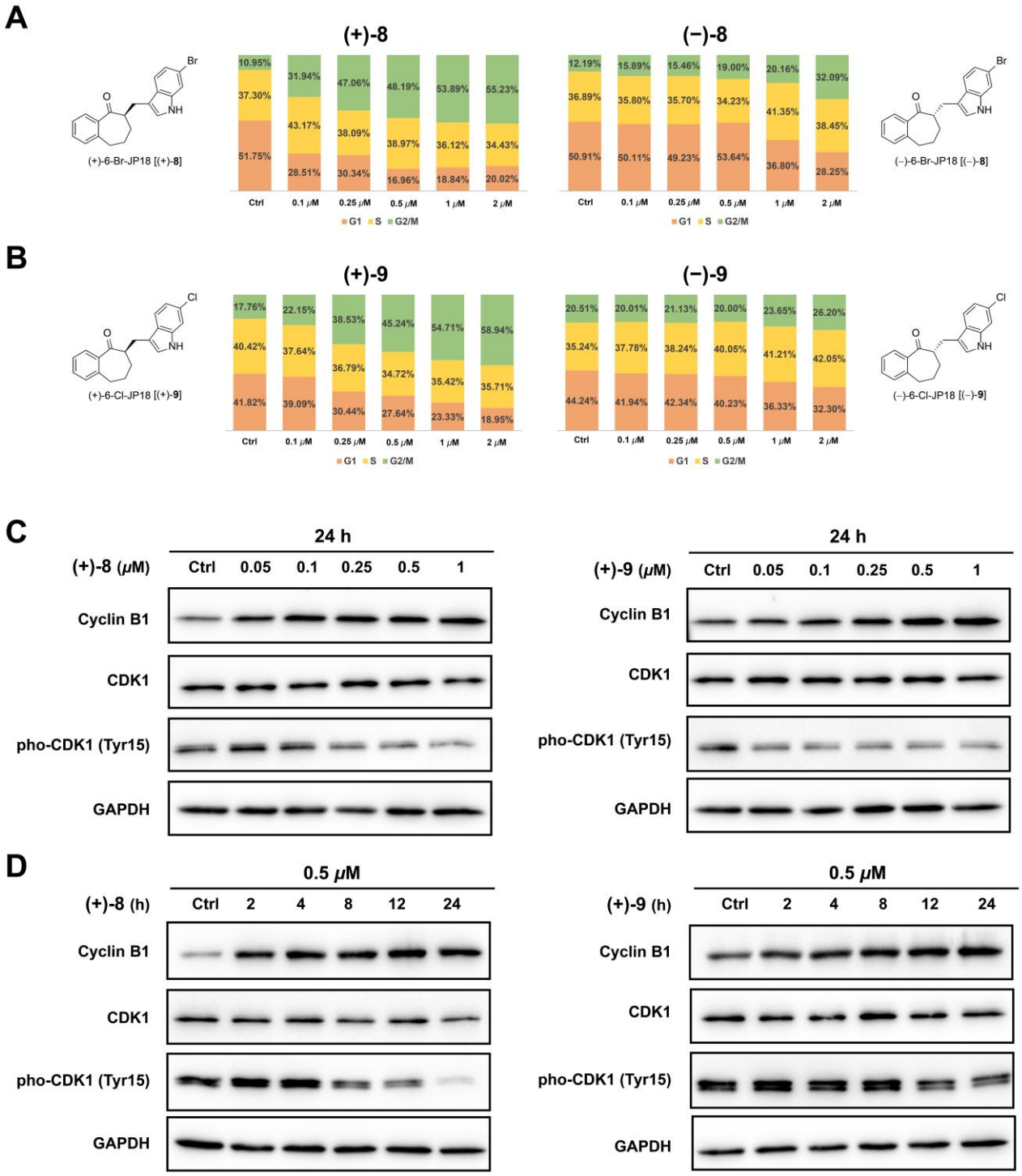

Figure 2. Determination of the enantiomeric forms of 6-Br-JP18 and 6-Cl-JP18 responsible for the cell cycle-arresting activity. (A) The cell cycle-arresting effect of the two enantiomers of 6-Br-JP18 (**8**). HeLa cells were treated with (+)-**8** and (−)-**8**, respectively, at the indicated concentrations for 8 h. (B) The cell cycle-arresting effect of the two enantiomers of 6-Cl-JP18 (**9**). HeLa cells were treated with (+)-**9** and (−)-**9**, respectively, at the indicated concentrations for 8 h. Bar graphs show the percentages of cells in the G2/M (green), S (yellow), and G1 (orange) phases. (C) Immunoblot analysis of G2/M phase markers in HeLa cells treated with (+)-**8** and (+)-**9**, respectively, at the indicated concentrations for 24 h. (D) Immunoblot analysis of G2/M phase markers in HeLa cells treated with (+)-**8** and (+)-**9**, respectively, at

0.50 μM for the indicated time periods. DMSO was used as a control for the compounds. GAPDH was used as a loading control in immunoblotting.

Compounds (+)-8 and (+)-9 disrupt the spindle microtubule assembly and arrest cell cycle in the M phase.

To understand their mode of action, we sought to specify whether (+)-**8** and (+)-**9** induce cell cycle arrest in the G2 phase or the M phase. Since the flow cytometry method described above could not differentiate between the two phases, key markers of mitosis were examined. Phosphorylation of histone H3 at Ser10 and Ser28 is associated with chromosome condensation, which lasts from prophase to metaphase of mitosis.[46] Both (+)-**8** and (+)-**9** increased the histone H3 phosphorylation levels in a dose- and time-dependent manner (Figures 3A and 3B). These results indicated that both (+)-**8** and (+)-**9** arrest cell cycle in the M phase. Immunofluorescence analysis showed that both (+)-**8** and (+)-**9** disrupted spindle microtubule assembly (Figure 3C). Notably, treatment with these compounds resulted in an uneven distribution of chromatids in the telophase of mitosis (Figures 3C8 and 3C12), which suggested a disruptive effect on the centromere organization and function.

Given their potent cytotoxicity, we examined a series of proteins associated with cell survival and death after treatment with (+)-**8** and (+)-**9**. In a dose-and time-dependent manner, the pro-survival protein B-cell lymphoma 2 (Bcl-2)[47] was downregulated, whereas the DNA damage marker phospho-histone H2AX (Ser139) (γ-H2AX)[48] was upregulated (Figure S5). Escalation of poly(ADP-ribose) polymerase 1 (PARP1) cleavage, a widely used marker of apoptosis,[49] was also observed with increasing dose and time (Figure S5). These results corroborated that (+)-**8** and (+)-**9** cause DNA damage and apoptosis.

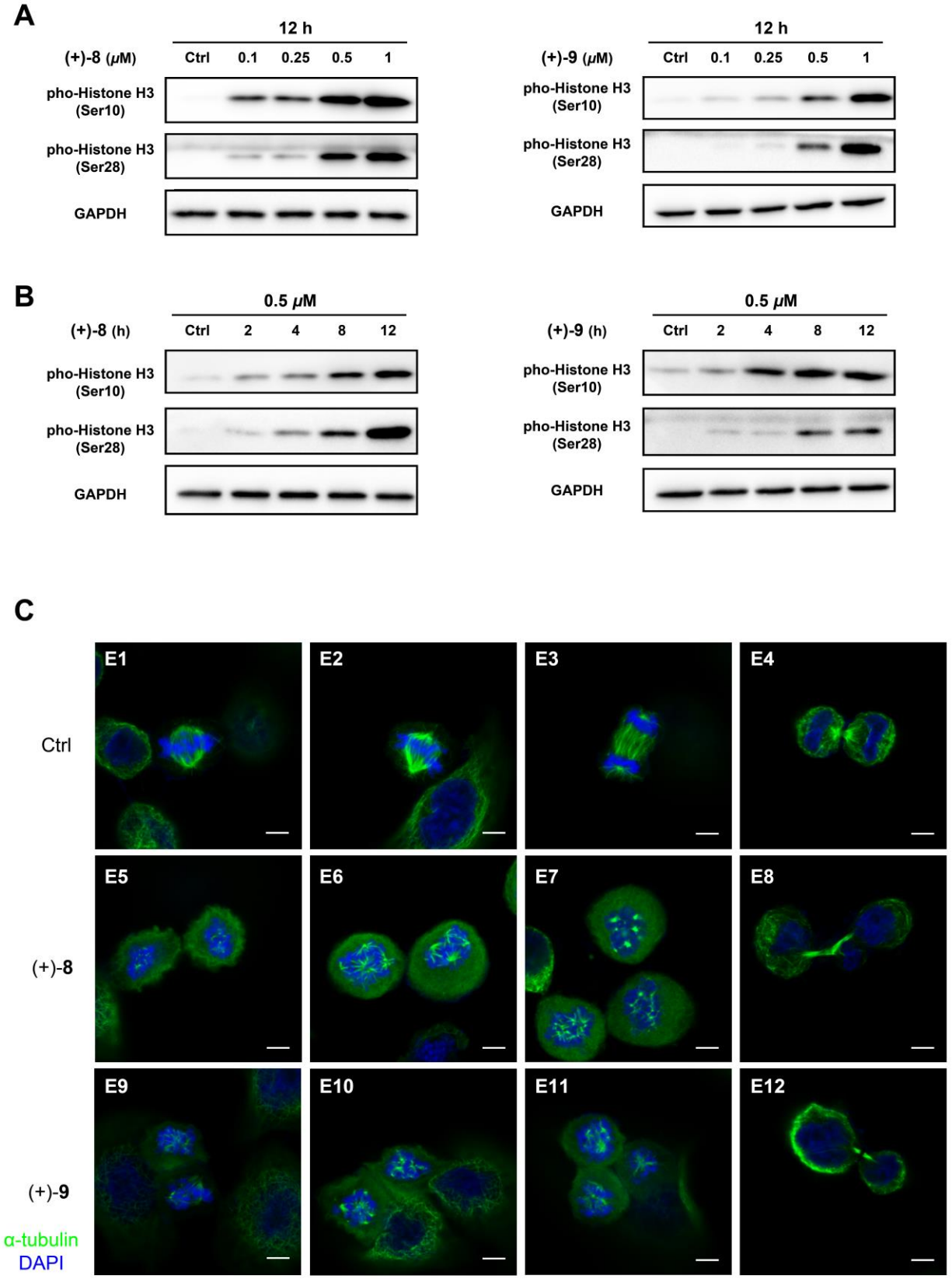

Figure 3. Effect of compounds (+)-8 and (+)-9 on M phase markers. (A) Immunoblot analysis of M phase markers in HeLa cells treated with (+)-**8** and (+)-**9**, respectively, at the indicated concentrations for 12 h. (B) Immunoblot analysis of M phase markers in HeLa cells treated with (+)-**8** and (+)-**9**, respectively, at 0.50 μM for the indicated time periods. DMSO was used as a control for the compounds. GAPDH was

used as a loading control in immunoblotting. (C) Immunofluorescence analysis of spindle microtubules and chromosomes in HeLa cells treated with (+)-**8** and (+)-**9**, respectively, at 100 nM for 8 h. The cells were stained with the α-tubulin antibody (green) and DAPI (blue). Scale bars indicate 5.0 μm.

Identification of α- and β-tubulins as potential protein targets of compounds (+)-8 and (+)-9.

The SAR study of JP18 demonstrated the difficulty in constructing a suitable small molecule probe for affinity-based target identification. Therefore, we resorted to the label-free method based on DARTS, which exploits the changes in the stability of the target protein against proteolysis due to the interaction with the small molecule.[50,51] Among the proteins identified by mass spectrometry, α- and β-tubulins were considered as potential targets of (+)-**8** (Figures 4A and 4B), given that this compound disrupts spindle microtubule assembly (Figure 3C). Immunoblotting analysis confirmed that both (+)-**8** and (+)-**9** decreased the stability of α- and β-tubulins (Figures 4C and 4D). To determine whether (+)-**8** binds directly to tubulin, we performed an in vitro tubulin polymerization assay. Similar to the reference compound nocodazole, (+)-**8** inhibited tubulin polymerization at a concentration of 5.0 μM (Figure 4E), which verified the direct interaction of this compound with tubulin.

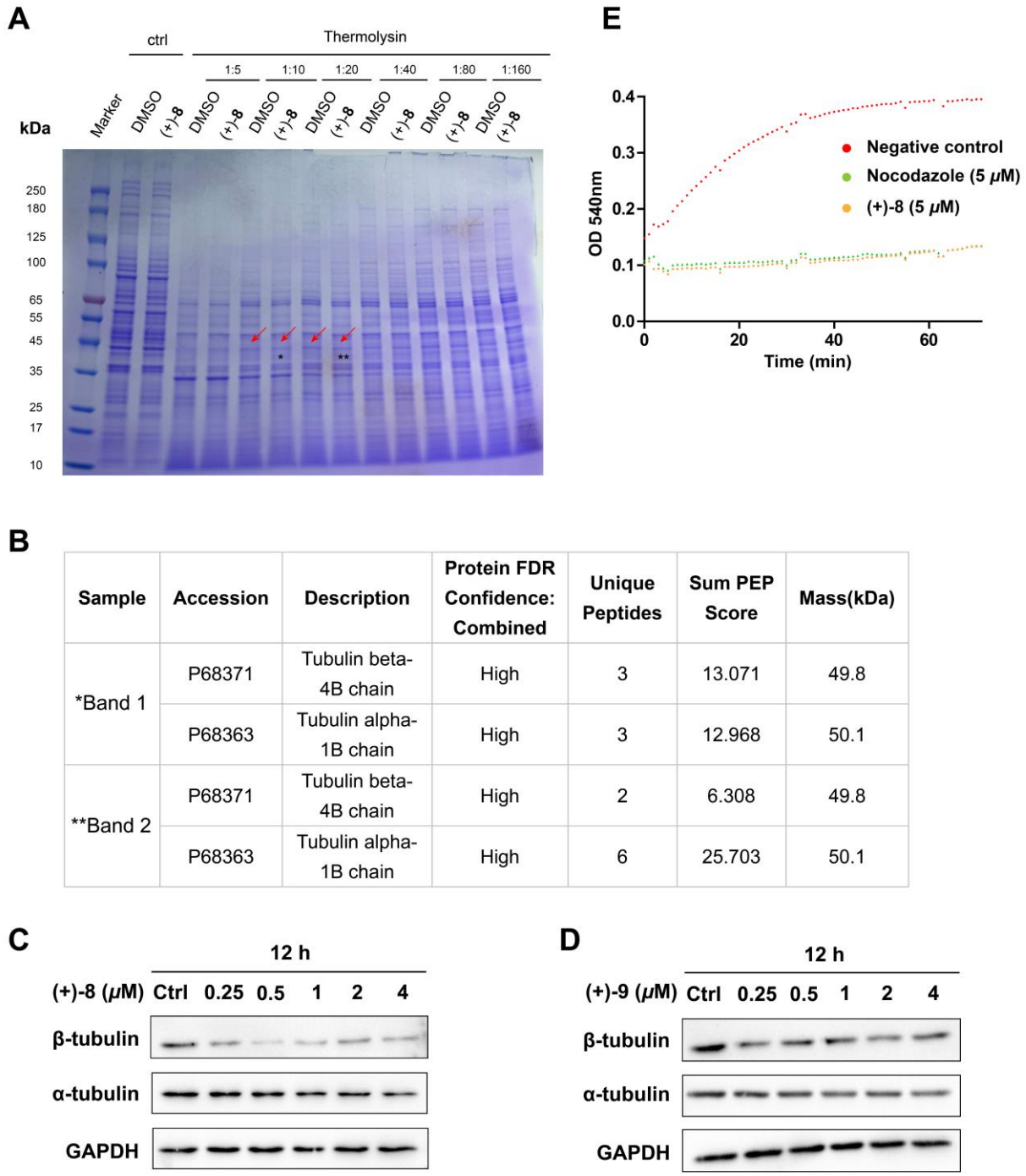

Sample	Accession	Description	Protein FDR Confidence: Combined	Unique Peptides	Sum PEP Score	Mass(kDa)
*Band 1	P68371	Tubulin beta-4B chain	High	3	13.071	49.8
	P68363	Tubulin alpha-1B chain	High	3	12.968	50.1
**Band 2	P68371	Tubulin beta-4B chain	High	2	6.308	49.8
	P68363	Tubulin alpha-1B chain	High	6	25.703	50.1

Figure 4. Identification of α- and β-tubulins as potential cellular targets of compound (+)-8. (A) A representative SDS-PAGE gel image showing the differential bands (~45 kDa; marked with red arrows) in the DARTS assay to identify the target(s) of (+)-**8**. HeLa cell lysates were treated with (+)-**8** (10 μM) for 1 h and then digested by thermolysin for 30 min. The asterisks indicate the bands that were subjected to mass spectrometry analysis. *Band 1. **Band 2. (B) Information on the potential protein targets of (+)-**8** identified by mass spectrometry. (C) Immunoblot analysis of α- and β-tubulins in HeLa cells treated with (+)-**8** at the indicated concentrations for 12 h. (D) Immunoblot analysis of α- and β-tubulins in HeLa cells treated with (+)-**9** at the indicated concentrations for 12 h. DMSO was used as the control for the compounds. (E) Inhibition of in vitro tubulin polymerization by (+)-**8**. The curves for (+)-**8** (5.0 μM), nocodazole (5.0 μM), and the control (DMSO) are shown in yellow, green, and red, respectively.

Compounds (+)-8 and (+)-9 bind to the colchicine-binding site of β-tubulin.

We investigated the details of the interaction between (+)-**8** and tubulin by X-ray crystallographic analysis. The compound was soaked into a complex of two αβ-tubulin heterodimers, the stathmin-like domain (SLD) of RB3, and tubulin tyrosine ligase (TTL) (the T2R−TTL complex).[52] The structure of the protein−ligand complex was refined at 2.5 Å resolution (PDB ID: 7CPD; see Table S1 for data collection and refinement statistics). As shown in Figure 5A, (+)-**8** occupies the colchicine-binding site of β-tubulin (Chain B and Chain D) at the intradimer interface. Protein−ligand interaction analysis using LigPlot[53] revealed the hydrophobic interaction of (+)-**8** with the following residues: β-Cys241, β-Leu242, β-Leu248, β-Ala250, β-Lys254, β-Leu255, β-Asn258, β-Met259, and β-Lys352 (Figure 5B). The indole N−H hydrogen atom forms a hydrogen bond with an oxygen atom of α-Thr179 (Figure 5B), which highlights the importance of the indole motif for binding to tubulin. The oxygen atom of the ketone forms a hydrogen bond with the N−H hydrogen atom of β-Asp251 (Figure 5B), which may explain the essential role of this oxygen atom observed in the SAR study (*vide supra*). The interaction of the bromine atom with β-Asn350 (Figure 5B) could further enhance the binding of (+)-**8** to β-tubulin,[54] which is consistent with the increased potency of this brominated analogue. The binding mode of (+)-**9** in the binding pocket of Chain B (PDB ID: 7CPQ) is essentially identical to that of (+)-**8**, although the binding of the chlorinated analogue to Chain D was not constructed due to insufficient electron density (Figure S6). Comparison of the MTA positions in the colchicine-binding pocket revealed that (+)-**8** and (+)-**9** are similar to colchicine (PDB ID: 4O2B) but different from nocodazole (PDB ID: 5CA1) (Figure 5C).

We then compared the structures of β-tubulin in the (+)-**8**-bound and unbound states. The side chains of Leu248 and Asn249 on the T7 loop of β-tubulin in the T2R−TTL complex (with αβ-tubulin in the curved conformation) occlude the colchicine-binding site (PDB ID: 4IIJ) (Figure 5D). In contrast, the T7 loop of β-tubulin in the T2R−TTL−(+)-**8** complex was found to flip outward to accommodate ligand binding (Figure 5D). Similar changes in the conformation of β-tubulin upon colchicine binding have been observed by Knossow and co-workers.[55] Furthermore, superimposition of the structure of (+)-**8**-bound β-tubulin and that of β-tubulin in the tubulin sheets (with αβ-tubulin in the straight conformation) (PDB ID:

1JFF) showed that (+)-**8** prevents the conversion of the curved conformation into the straight conformation by altering the conformations of the T7 loop, H7, H8, S8, and S9, thereby disrupting proper microtubule assembly. This is the characteristic molecular mechanism of action of colchicine-binding site inhibitors (CBSIs).[56]

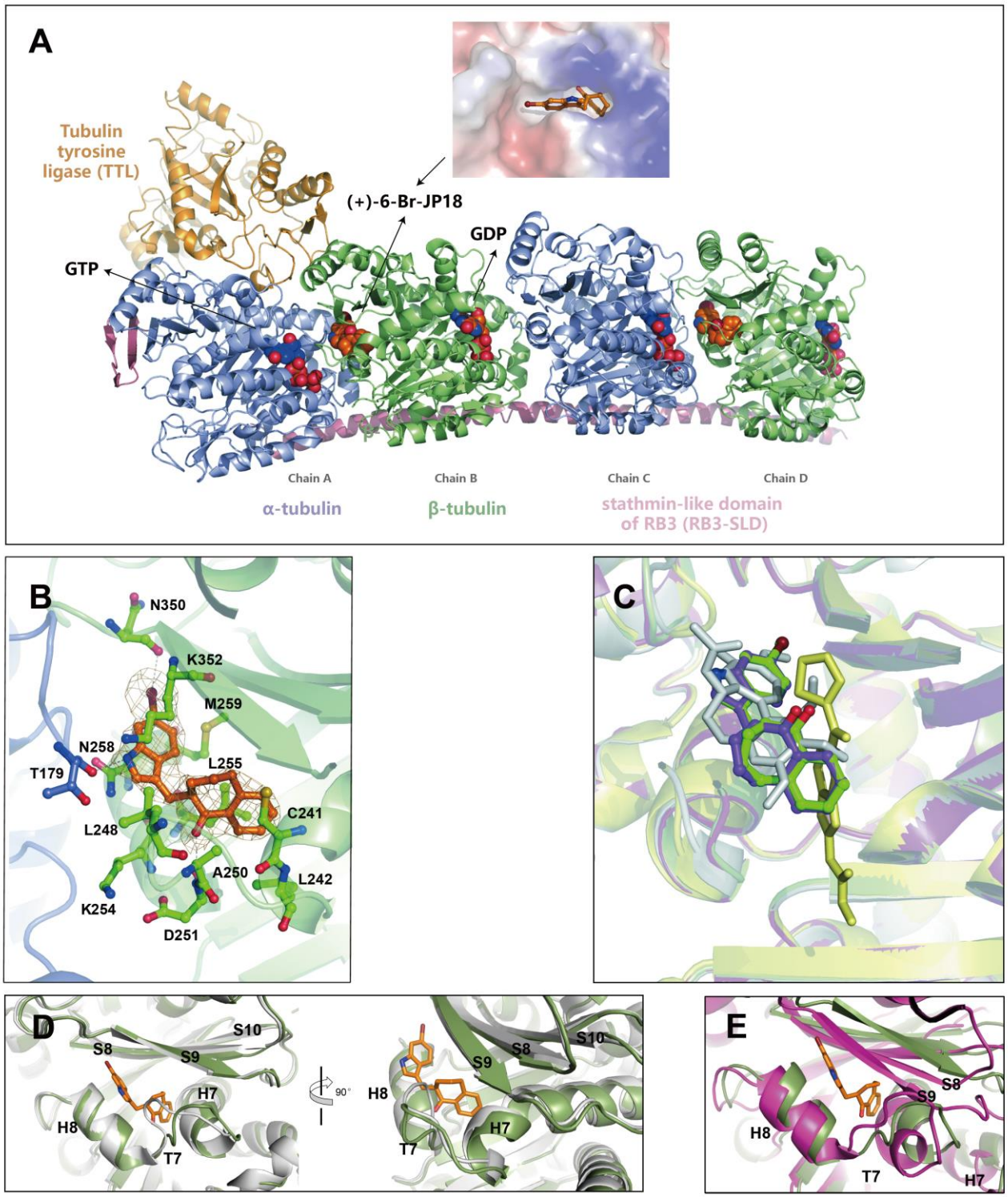

Figure 5. X-ray crystal structure of the T2R-TTL tubulin−(+)-8 complex. (A) Overall structure of the T2R−TTL−(+)-**8** complex. α-Tubulin (light slate blue), β-tubulin (green), RB3-SLD (plum), and TTL (gold) are shown in cartoon representation. Compound (+)-**8**, GDP, and GTP are shown in sphere representation. (B) Close-up view of the interaction between (+)-**8** and the colchicine-binding site of β-tubulin. α-Tubulin and β-tubulin are colored in light slate blue and green, respectively. The Fo−Fc simulated annealing omit map (contoured at 1.0 σ) is shown as a mesh. The residues involved in the interaction between (+)-**8** and β-tubulin are shown in stick representation. The hydrogen and halogen bonds are shown as dashed lines. (C) Comparison of the position of (+)-**8**/(+)-**9** with those of colchicine and nocodazole in the colchicine-binding pocket. The four T2R-TTL-CBSI complex structures are superimposed, and (+)-**8** (green), (+)-**9** (medium purple), colchicine (gray), and nocodazole (yellow) are shown in stick representation. (D) Superimposition of the structure of (+)-**8**-bound β-tubulin (green) and that of unbound β-tubulin in the T2R−TTL complex (with αβ-tubulin in the curved conformation) (gray). (E) Superimposition of the structure of (+)-**8**-bound β-tubulin (green) and that of unbound β-tubulin in the tubulin sheets (with αβ-tubulin in the straight conformation) (violet red).

Compounds (+)-8 and (+)-9 suppress the ubiquitin-mediated proteolysis of CENP-A.

Having noticed the uneven distribution of chromatids induced by (+)-**8** and (+)-**9** (Figure 3C), we postulated that these compounds may affect centromere positioning, which is determined by the deposition of CENP-A.[17–19] Therefore, the effect of (+)-**8** and (+)-**9** on CENP-A levels was investigated. Both compounds upregulated CENP-A in HeLa cells in a dose- and time-dependent manner [(+)-**8**: Figures 6A and 6F; (+)-**9**: Figures 6B and 6G]. To further understand the relationship between microtubule assembly and CENP-A regulation, we tested a number of other MTAs. Interestingly, not only the microtubule destabilizers nocodazole and vinblastine but also the microtubule stabilizer paclitaxel increased CENP-A levels in a dose- and time-dependent manner (Figures 6C–6E and Figures 6H–6J). These results indicated a significant correlation between microtubule assembly and CENP-A regulation in mitosis.

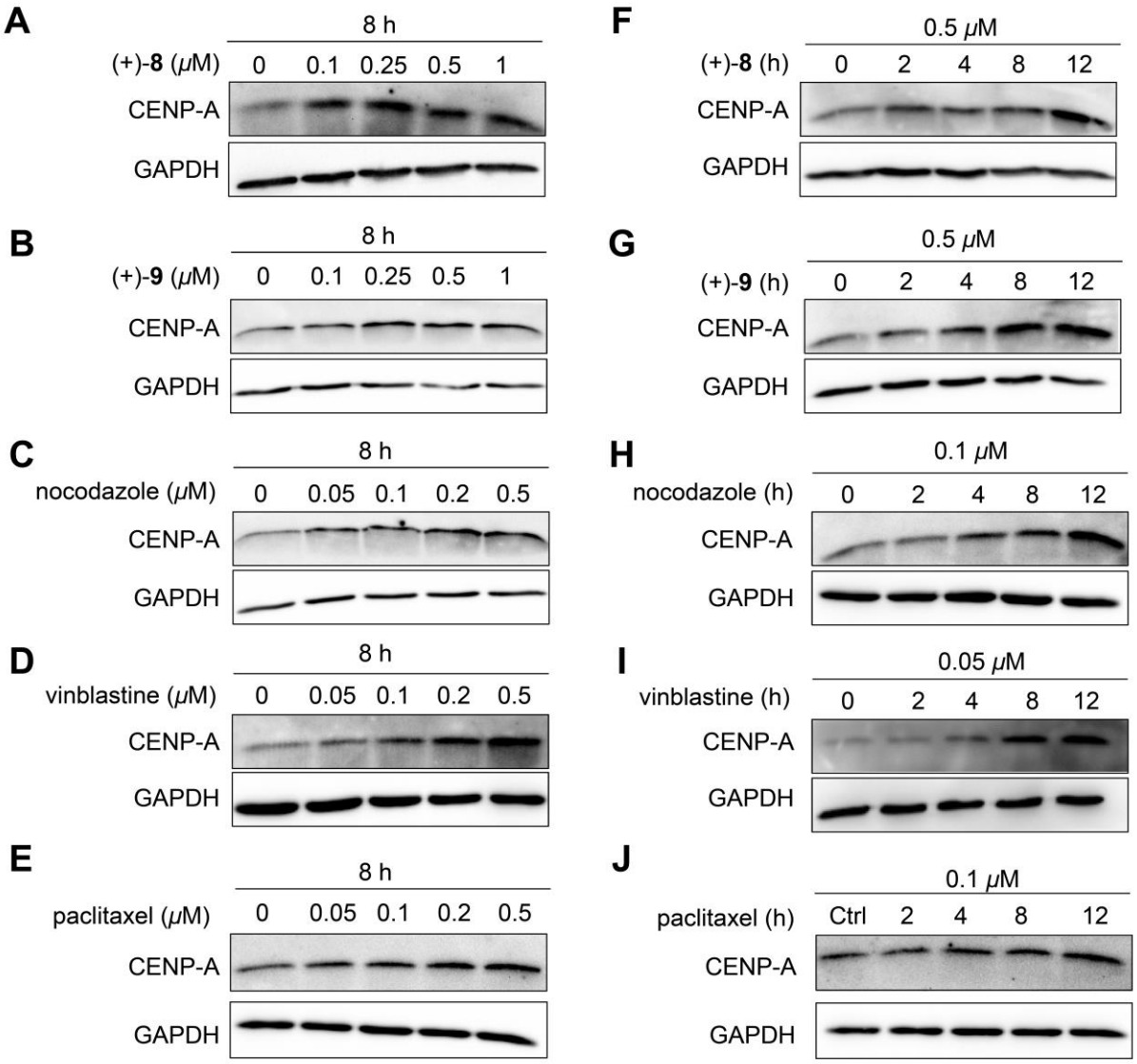

Figure 6. MTAs upregulated CENP-A. (A–E) Immunoblot analysis of CENP-A in HeLa cells treated with (+)-**8**, (+)-**9**, nocodazole, vinblastine, and paclitaxel, respectively, at the indicated concentrations for 8 h. (F–J) Immunoblot analysis of CENP-A in HeLa cells treated with (+)-**8** (0.50 μM), (+)-**9** (0.50 μM), nocodazole (0.10 μM), vinblastine (0.050 μM), and paclitaxel (0.10 μM), respectively, for the indicated time periods. DMSO was used as a control for the compounds. GAPDH was used as a loading control in immunoblotting.

We further determined whether MTAs affect CENP-A at the transcriptional or post-translational level. Real-time PCR analysis showed that the tested MTAs had no influence on the CENP-A mRNA levels in HeLa cells (Figure 7A). Therefore, we focused our attention on the post-translational regulation of CENP-A, which may be mediated by the ubiquitin-proteasome system (UPS) and/or the lysosome system. The proteasome inhibitor MG132 was found to increase CENP-A protein levels in HeLa cells (Figures 7B and 7C), whereas the lysosome inhibitors NH_4Cl (Figure S7A) and chloroquine (CQ) (Figure S7B) had

essentially no effect. Furthermore, overexpression of ubiquitin (Ub) resulted in downregulation of CENP-A (Figures 7D and 7E), whereas overexpression of the ubiquitin-like proteins[57] neural precursor cell-expressed developmentally downregulated protein 8 (NEDD8) (Figure S7C) and small ubiquitin like modifier 1 (SUMO1) (Figure S7D) had no such effect. These observations suggested that ubiquitin-mediated proteolysis is the primary means of CENP-A degradation in mitosis. The effect of MTAs on the proteolysis of CENP-A was then investigated. The CENP-A levels in HeLa cells treated with the MTA alone and in those co-treated with the MTA and MG132 were compared by immunoblot analysis. Compared to (+)-**8** alone and MG132 alone, the combination of (+)-**8** and MG132 did not further increase the CENP-A levels (Figures 7F and 7G). Similar observations were made with (+)-**9** (Figures 7H and 7I) and nocodazole (Figure S7E). These results indicated that the tested MTAs act on the same CENP-A degradation system as the proteasome inhibitor.

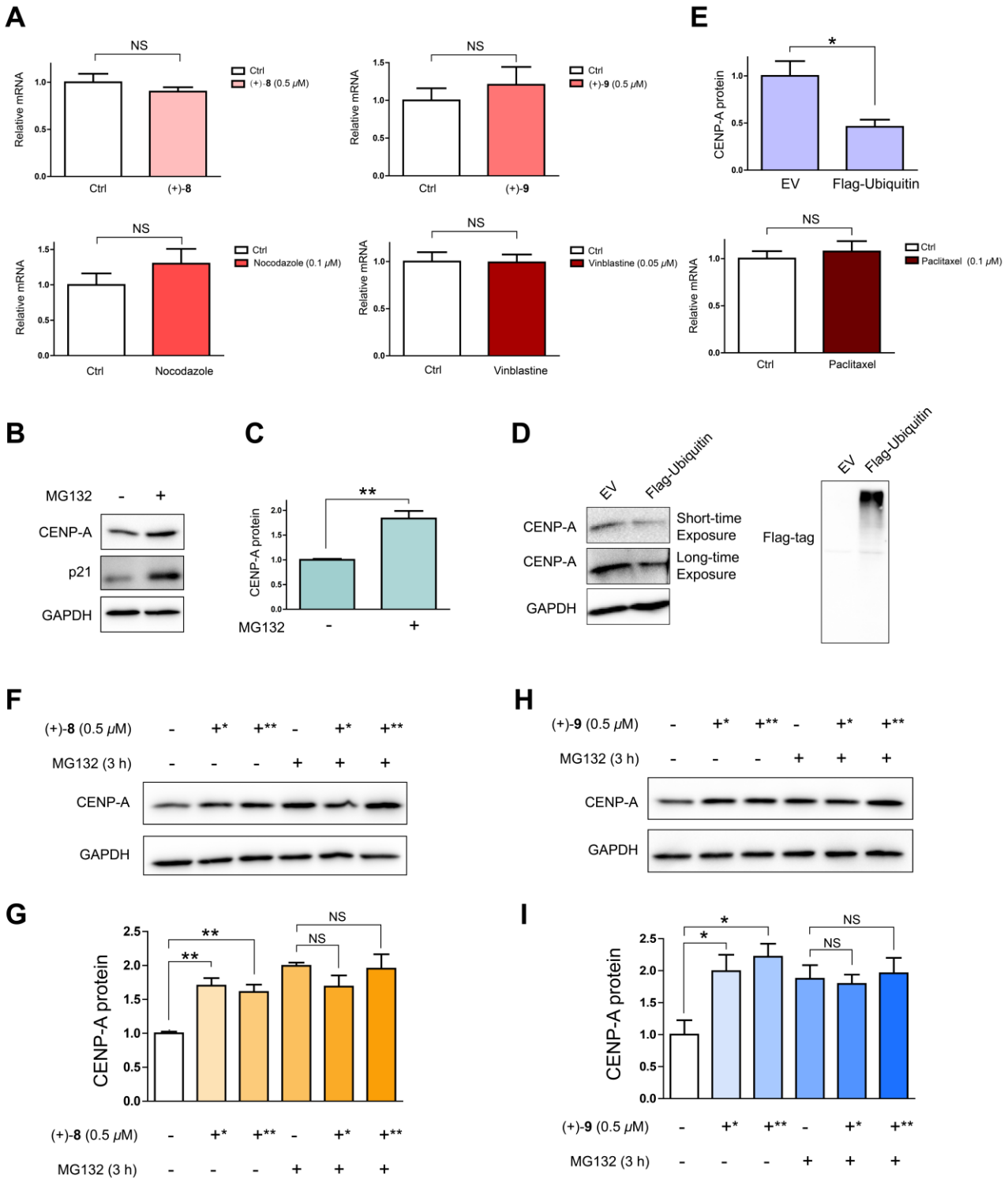

Figure 7. Compounds (+)-8 and (+)-9 suppress the degradation of CENP-A by inhibiting the ubiquitin-proteasome system. (A) qRT-PCR analysis of the mRNA levels of CENP-A in HeLa cells treated with (+)-**8** (0.50 μM), (+)-**9** (0.50 μM), nocodazole (0.10 μM), vinblastine (0.050 μM), and paclitaxel (0.10 μM), respectively, for 6 h. The mRNA levels of β-actin were used as the reference for normalization. Data are representative of three independent biological replicates and are presented as mean ± s.e.m. NS = not significant (significance level: $\alpha = 0.05$; $n = 3$, two-tailed Student's *t*-test). (B) Immunoblot analysis of CENP-A in HeLa cells treated with MG132 (50 μM) for 3 h. p21 served as a

positive control. (C) Quantitative analysis of the immunoblotting data of CENP-A obtained from the above experiment. Data are representative of three independent biological replicates and are presented as mean ± s.e.m. $^{**}P < 0.01$ ($n = 3$, two-tailed Student's *t*-test). (D) Immunoblot analysis of CENP-A in HeLa cells transfected with FLAG-ubiquitin. (E) Quantitative analysis of the immunoblotting data of CENP-A obtained from the above experiment. Data are representative of three independent biological replicates and are presented as mean ± s.e.m. $^{*}P < 0.05$ ($n = 3$, two-tailed Student's *t*-test). (F) Comparison of the CENP-A levels in HeLa cells treated with (+)-**8** (0.50 μM) and co-treated with (+)-**8** (0.50 μM) and MG-132 (50 μM) for the indicated time periods by immunoblotting. *4 h. **6 h. (G) Quantitative analysis of the immunoblotting data of CENP-A obtained from the above experiment. Data are representative of three independent biological replicates and are presented as mean ± s.e.m. $^{**}P < 0.01$, NS = not significant ($n = 3$, two-tailed Student's *t*-test). (H) Comparison of the CENP-A levels in HeLa cells treated with (+)-**9** (0.50 μM) and co-treated with (+)-**9** (0.50 μM) and MG-132 (50 μM) for the indicated time periods by immunoblotting. *4 h. **6 h. (I) Quantitative analysis of the immunoblotting data of CENP-A obtained from the above experiment. Data are representative of three independent biological replicates and are presented as mean ± s.e.m. $^{*}P < 0.05$, NS = not significant ($n = 3$, two-tailed Student's *t*-test). DMSO was used as a control for the compounds. GAPDH was used as a loading control in immunoblotting.

Compound (+)-8-Induced upregulation of CENP-A is mediated by destabilizing Cdh1 subunit of E3 ubiquitin ligase APC/C.

APC/C (anaphase-promoting complex/cyclosome) is an important E3 ligase in the regulation of mitosis, the substrate selectivity of which is determined by its co-activators Cdh1 and Cdc20.[58,59] Notably, the APC/C complexes were found to participate in the regulation of CENP-A in *Drosophila*; CENP-A^{CID} increased upon Cdh1 or Cdc20 depletion.[60] In addition to the APC/C complexes, the Cullin−RING E3 ubiquitin ligase (CRL) complexes also proved to be relevant to the CENP-A regulation. In Hela cells, CUL4-DDB1-DCAF11 E3 ligase complex mediated degradation of CENP-A via poly-ubiquitylation,[27] and CUL4A-RBX1-COPS8 E3 ligase complex directed CENP-A deposition via mono-ubiquitylation.[28] In view of these reports, we sought to identify the E3 ligase(s) involved in MTA-induced upregulation of CENP-A.

We first examined whether APC/C co-activators were associated with MTA-induced upregulation of CENP-A. Treatment of HeLa cells with (+)-**8** (Figures 8A and 8B) or paclitaxel (Figures 8C and 8D) resulted in a time-dependent decrease in Cdh1 levels and a time-dependent increase in CENP-A levels. In contrast, Cdc20 remained unaffected upon treatment with (+)-**8** or paclitaxel (Figures 8A and 8C). Similar observations in human hepatocellular carcinoma Hep G2 cells, human lung carcinoma A549 cells, and human normal liver L-02 cells (Figure S8) suggested that Cdh1 downregulation generally correlates with

MTA-induced CENP-A upregulation. By comparing the Cdh1 degradation rates in HeLa cells treated with the protein synthesis inhibitor cycloheximide (CHX) alone and co-treated with (+)-**8** and CHX, we found that Cdh1 was downregulated by (+)-**8** at the post-translational level. (Figure S9). Notably, overexpression of the Flag-Cdh1 construct counteracted the effect of (+)-**8** on the CENP-A level in HeLa cells (Figures 8E and 8F). Furthermore, siRNA-mediated knockdown of Cdh1 in Hela cells led to upregulation of CENP-A, rather than its homologue histone H3 (Figures 8G and 8H). In contrast, knockdown of Cdc20 had essentially no effect on the CENP-A level (Figures 8I and 8J). Similar correlations between Cdh1 depletion and CENP-A upregulation in Hep G2, A549, human triple-negative breast cancer MDA-MB-231, human glioblastoma U251, and L-02 cells (Figure S10) revealed that Cdh1 is responsible for CENP-A regulation from a general perspective. We then compared the rates of CENP-A degradation in Cdh1-knockdown and non-knockdown HeLa cells treated with CHX (Figure 8K). The significantly lower rate in the Cdh1-knockdown cells indicated that the Cdh1 depletion mediated the upregulation of CENP-A at the post-translational level. The combination of Cdh1 knockdown and MTA treatment resulted in increased CENP-A accumulation compared to MTA treatment alone (Figures S11A and S11B). This suggested that Cdh1 functioned at the prometaphase of mitosis, the stage at which MTA-treated cells were arrested.

We then investigated whether DCAF11, a key component of the CUL4-DDB1-DCAF11 E3 ligase complex, was involved in MTA-induced CENP-A upregulation. The Cullin 4A and DCAF11 levels in HeLa cells were unaffected upon treatment with (+)-**8** (Figure S12A) or paclitaxel (Figure S12B). Compared to treatment with the MTA alone, the combination of DCAF11 knockdown and treatment with either MTA did not further upregulate CENP-A (Figures S11C and S11D). These results indicated that DCAF11 was not responsible for CENP-A degradation in prometaphase of mitosis.

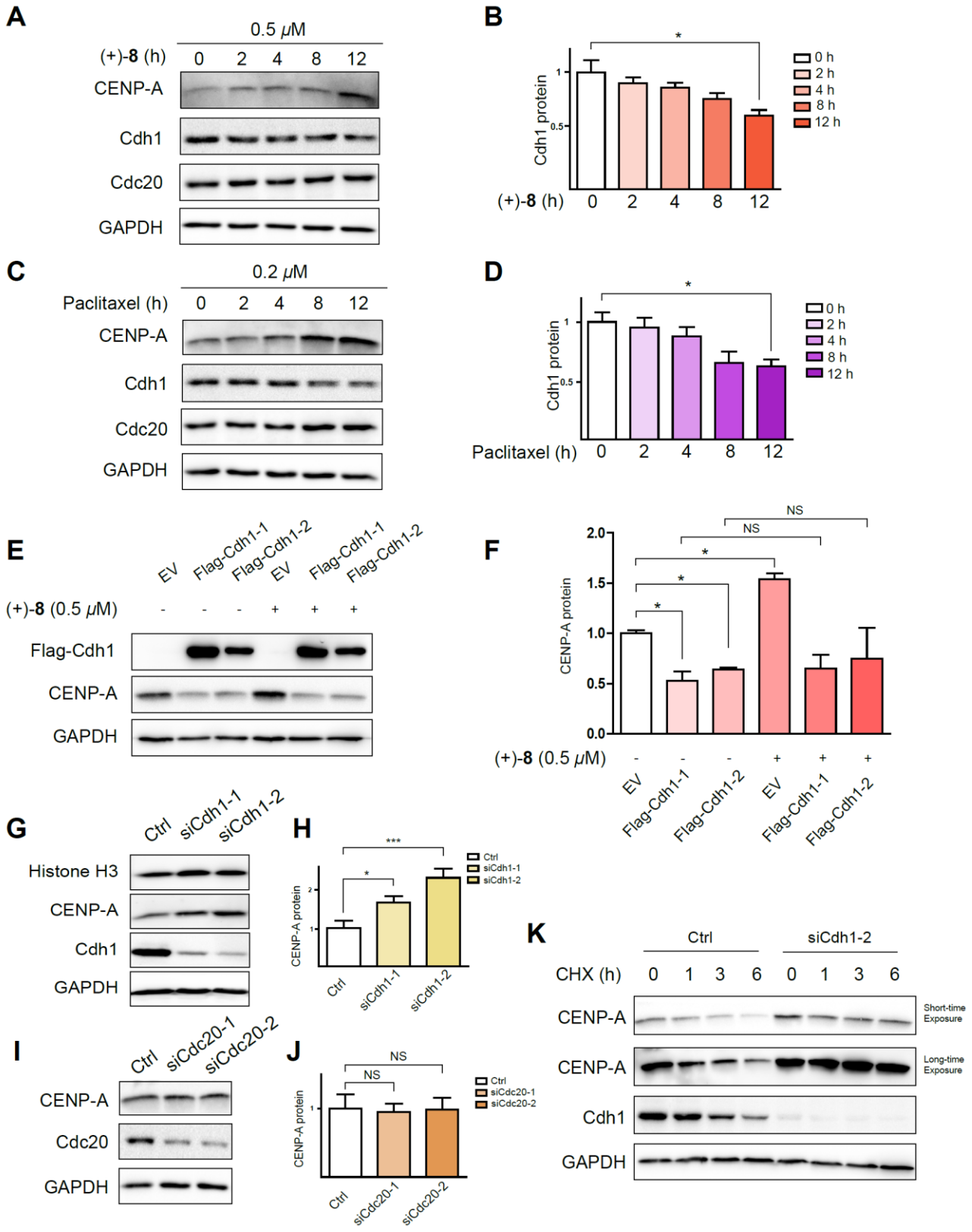

Figure 8. Compound (+)-8 destabilizes Cdh1 to upregulate CENP-A. (A) Immunoblot analysis of CENP-A, Cdh1, and Cdc20 in HeLa cells treated with (+)-**8** (0.50 μM) for the indicated time periods. (B) Quantitative analysis of the immunoblotting data of Cdh1 obtained from the above experiment. Data are representative of three independent biological replicates and are presented as mean ± s.e.m. *$P < 0.05$ ($n = 3$, two-tailed Student's t-test). (C) Immunoblot analysis of CENP-A, Cdh1, and Cdc20 in HeLa cells treated with paclitaxel (0.20 μM) for the indicated time periods. (D) Quantitative analysis of the

immunoblotting data of Cdh1 obtained from the above experiment. Data are representative of three independent biological replicates and are presented as mean ± s.e.m. *$P < 0.05$ ($n = 3$, two-tailed Student's *t*-test). (E) Immunoblot analysis of CENP-A in HeLa cells transfected with FLAG-Cdh1 and then treated with (+)-**8** (0.50 μM) for 12 h. Cdh1-1 and Cdh1-2 represent human Cdh1 isoform 1 (Q9UM11-2) and isoform 2 (Q9UM11-1), respectively. (F) Quantitative analysis of the immunoblotting data obtained from the above experiment. Data are representative of three independent biological replicates and are presented as mean ± s.e.m. *$P < 0.05$, NS = not significant ($n = 3$, two-tailed Student's *t*-test). (G) Immunoblot analysis of CENP-A in HeLa cells transfected with siRNA targeting Cdh1 mRNA. (H) Quantitative analysis of the immunoblotting data obtained from the above experiment. Data are representative of three independent biological replicates and are presented as mean ± s.e.m. *$P < 0.05$, ***$P < 0.001$ ($n = 3$, two-tailed Student's *t*-test). (I) Immunoblot analysis of CENP-A in HeLa cells transfected with siRNA targeting Cdc20 mRNA. (J) Quantitative analysis of the immunoblotting data obtained from the above experiment. Data are representative of three independent biological replicates and are presented as mean ± s.e.m. NS = not significant ($n = 3$, two-tailed Student's *t*-test). (K) Immunoblot analysis of CENP-A in HeLa cells transfected with siRNA targeting Cdh1 mRNA and then treated with cycloheximide (CHX) for the indicated time periods.

Discussion

Taking advantage of the DARTS-based method, we identified β-tubulin as a cellular target of the cell cycle inhibitors (+)-6-Br-JP18 and (+)-6-Cl-JP18; the interaction between β-tubulin and the small molecules was further verified by X-ray crystallographic analysis. Notably, this class of compounds was significantly less potent after chemical labeling and therefore not amenable to the affinity chromatography-based-target identification. In this case, DARTS demonstrated its simplicity and convenience as a label-free method for target identification.

Maintenance of centromeric identity requires precise deposition of CENP-A.[14–16] Aberrant overexpression of CENP-A, which leads to its mislocalization, is associated with the malignant potential of tumors.[21–24] Therefore, understanding of the regulatory mechanisms of CENP-A expression and degradation would provide insight into cancer development and benefit cancer therapy. Ubiquitin-mediated proteolysis of CENP-A has emerged as a common mechanism to regulate its stability and prevent ectopic assembly of CENP-A chromatin across species.[25,26] In *Drosophila*, the E3 ubiquitin ligases APC/C^{Cdh1} and SCF^{Ppa} were found to be responsible for the ubiquitin-mediated proteolysis of centromere identifier (CID; the *Drosophila* orthologue of CENP-A) in G1 phase and G1 and S phases, respectively.[60] We discovered that Cdh1 regulates CENP-A in a "necessary and sufficient" manner (Figures 8E–8H) in mitosis of human cells, which links spindle formation and CENP-A modulation.

Although an effective class of chemotherapeutic agents, MTAs can induce drug resistance and disease relapse after long-term use.[7,61] An important mechanism contributing to this resistance is that cancer cells evade drug-induced mitotic arrest to avoid subsequent cell death.[7,8] This process, also known as mitotic slippage, is closely associated with aneuploidy and CIN,[8] which are thought to result from aberrant overexpression of CENP-A.[19,20] Our discovery that disruption of spindle microtubule assembly with MTAs significantly upregulated CENP-A (Figure 6) fills a gap in the possible mechanism for the MTA-induced drug resistance. This study suggests a potential role for Cdh1 in preventing the emergence of MTA-induced drug resistance in cancer therapy.

Acknowledgments

This paper is dedicated to the memory of Prof. Hualiang Jiang. We thank Prof. Kuiling Ding, Prof. Xin Zhang, and Fahui Zhu for discussion. We thank Biomedical Science at Fudan University and Shanghai Synchrotron Radiation Facility for technical assistance. This work was supported by National Natural Science Foundation of China (21572064, 21931014, 21772225, and U2002221), Ministry of Science and Technology of China (2018YFA0901900), Chinese Academy of Sciences (121731KYSB20190039 and QYZDB-SSW-SLH040), and Science and Technology Commission of Shanghai Municipality (JCYJ-SHFY-2022-005 and 20430713400). A.L. is grateful to Tencent Foundation.

References

1. Mitchison, T.J. and Salmon, E. D. (2001). Mitosis: a history of division. Nat. Cell Biol. *3*, E17–E21

2. McIntosh, J.R. (2016). Mitosis. Cold Spring Harb. Perspect. Biol. *8*, a023218.

3. Compton, D.A. (2000). Spindle assembly in animal cells. Annu. Rev. Biochem. *69*, 95–114.

4. Gudimchuk, N.B. and McIntosh, J.R. (2021). Regulation of microtubule dynamics, mechanics and function through the growing tip. Nat. Rev. Mol. Cell Biol. *22*, 777–795.

5. M.A. Jordan and L. Wilson (2004). Microtubules as a target for anticancer drugs. Nat. Rev. Cancer *4*, 253–265.

6. Cermak, V., Dostal, V., Jelinek, M., Libusova, L., Kovar, J., Rosel, D., and Brabek, J. (2020). Microtubule-targeting agents and their impact on cancer treatment. Eur. J. Cell Biol. *99*, 151075.

7. Cheng, B. and Crasta, K. (2017). Consequences of mitotic slippage for antimicrotubule drug therapy. Endocr. Relat. Cancer *24*, T97–T106.

8. Sinha, D., Duijf, P.H.G., and Khanna, K.K. (2019). Mitotic slippage: an old tale with a new twist. Cell Cycle *18*, 7–15.

9. McClelland, S.E., Burrell, R.A., and Swanton, C. (2009). Chromosomal instability: a composite phenotype that influences sensitivity to chemotherapy. Cell Cycle *8*, 3262–3266.

10. Vishwakarma, R. and McManus, K.J. (2020). Chromosome Instability; implications in cancer development, progression, and clinical outcomes. Cancers *12*, 824.

11. Lukow, D.A. and Sheltzer, J.M. (2022). Chromosomal instability and aneuploidy as causes of cancer drug resistance. Trends Cancer *8*, 43–53.

12. Ippolito, M.R., Martis, V., Martin, S., Tijhuis, A.E., Hong, C., Wardenaar, R., Dumont, M., Zerbib, J., Spierings, D.C.J., Fachinetti, D., Ben-David, U., Foijer, F., Santaguida, S. (2021). Gene copy-number changes and chromosomal instability induced by aneuploidy confer resistance to chemotherapy. Dev. Cell *56*, 2440–2454.

13. Reploglea, J.M., Zhou, W., Amaroa, A.E., McFarlandc, J.M., Villalobos-Ortizd, M., Ryan, J., Letai, A., Yilmaz, O., Sheltzer, J., Lippard, S.J., Ben-David, U., and Amon, A. (2020). Aneuploidy increases resistance to chemotherapeutics by antagonizing cell division. Proc. Natl. Acad. Sci. USA *117*, 30566–30576.

14. Black, B.E. and Bassett, E.A. (2008). The histone variant CENP-A and centromere specification. Curr. Opin. Cell Biol. *20*, 91–100.

15. De Rop, V., Padeganeh, A., and Maddox, P.S. (2012). CENP-A: the key player behind centromere identity, propagation, and kinetochore assembly. Chromosoma *121*, 527–538.

16. Kixmoeller, K., Allu, P.K., and Black, B.E. (2020). The centromere comes into focus: from CENP-A nucleosomes to kinetochore connections with the spindle. Open Biol. *10*, 200051.

17. Chen, C.C. and Mellone, B.G. (2016). Chromatin assembly: Journey to the CENter of the chromosome. J. Cell Biol. *214*, 13–24.

18. McKinley, K.L. and Cheeseman, I.M. (2016). The molecular basis for centromere identity and function. Nat. Rev. Mol. Cell Biol. *17*, 16–29.

19. Mahlke, M.A. and Nechemia-Arbely, Y. (2020). Guarding the genome: CENP-A-chromatin in health and cancer. Genes *11*, 810.

20. Shrestha, R.L., Ahn, G.S., Staples, M.I., Sathyan, K.M., Karpova, T.S., Foltz, D.R., and Basrai, M.A. (2017). Mislocalization of centromeric histone H3 variant CENP-A contributes to chromosomal instability (CIN) in human cells. Oncotarget *8*, 46781–46800.

21. Zink, L.M. and Hake, S.B. (2016). Histone variants: nuclear function and disease. Curr. Opin. Genet. Dev. *37*, 82–89.

22. Sharma, A.B., Dimitrov, S., Hamiche, A., and Van Dyck, E. (2019). Centromeric and ectopic assembly of CENP-A chromatin in health and cancer: old marks and new tracks. Nucleic Acids Res. *47*, 1051–1069.

23. McGovern, S.L., Qi, Y., Pusztai, L., Symmans, W.F., and Buchholz, T.A. (2012). Centromere protein-A, an essential centromere protein, is a prognostic marker for relapse in estrogen receptor-positive breast cancer. Breast Cancer Res. *14*, R72.

24. Sun, X., Clermont, P.-L., Jiao, W., Helgason, C.D., Gout, P.W., Wang, Y., and Qu, S. (2016). Elevated expression of the centromere protein-A(CENP-A)-encoding gene as a prognostic and predictive biomarker in human cancers. Int. J. Cancer *139*, 899–907.

25. Niikura, Y., Kitagawa, R., and Kitagawa, K. (2017). CENP-A Ubiquitylation Is Required for CENP-A Deposition at the Centromere. Dev. Cell *40*, 7–8.

26. Srivastava, S. and Foltz, D.R. (2018). Posttranslational modifications of CENP-A: marks of distinction. Chromosoma *127*, 279–290.

27. Wang, K., Liu, Y., Yu, Z., Gu, B., Hu, J., Huang, L., Ge, X., Xu, L., Zhang, M., Zhao, J., Hu, M., Le, R., Wu, Q., Ye, S., Gao, S., Zhang, X., Xu, R.M., and Li, G. (2021). Phosphorylation at Ser68 facilitates DCAF11-mediated ubiquitination and degradation of CENP-A during the cell cycle. Cell Rep. *37*, 109987.

28. Niikura, Y., Kitagawa, R., Ogi, H., Abdulle, R., Pagala, V., and Kitagawa, K. (2015). CENP-A K124 ubiquitylation is required for CENP-A deposition at the centromere. Dev. Cell *32*, 589–603.

29. Marcos, I.S., Moro, R.F., Costales, I., Basabe, P., and Diez, D. (2013). Sesquiterpenyl indoles. Nat. Prod. Rep. *30*, 1509–1526.

30. Corsello, M.A., Kim, J., and Garg, N.K. (2017). Indole diterpenoid natural products as the inspiration for new synthetic methods and strategies. Chem. Sci. *8*, 5836–5844.

31. Devi, N., Kaur, K., Biharee, A., and Jaitak, V. (2021). Recent development in indole derivatives as anticancer agent: a mechanistic approach. Anticancer Agents Med. Chem. *21*, 1802–1824.

32. Sravanthi, T.V. and Manju, S.L. (2016). Indoles — A promising scaffold for drug development. Eur. J. Pharm. Sci. *91*, 1–10.

33. Sallam, A.A., Ayoub, N.M., Foudah, A.I., Gissendanner, C.R., Meyer, S.A., and El Sayed, K.A. (2013). Indole diterpene alkaloids as novel inhibitors of the Wnt/beta-catenin pathway in breast cancer cells. Eur. J. Med. Chem. *70*, 594–606.

34. Sallam, A.A., Houssen, W.E., Gissendanner, C.R., Orabi, K.Y., Foudah, A.I., and El Sayed, K.A. (2013). Bioguided discovery and pharmacophore modeling of the mycotoxic indole diterpene alkaloids penitrems as breast cancer proliferation, migration, and invasion inhibitors. MedChemComm *4*, 1360–1369.

35. Goda, A.A., Siddique, A.B., Mohyeldin, M., Ayoub, N.M., and El Sayed, K.A. (2018). The Maxi-K (BK) channel antagonist Penitrem A as a novel breast cancer-targeted therapeutic. Mar. Drugs. *16*, 157.

36. Sun, Y., Li, R., Zhang, W., and Li, A. (2013). Total synthesis of indotertine A and drimentines A, F, and G. Angew. Chem. Int. Ed. *52*, 9201–9204.

37. Sun, Y., Chen, P., Zhang, D., Baunach, M., Hertweck, C., and Li, A. (2014). Bioinspired total synthesis of sespenine. Angew. Chem. Int. Ed. *53*, 9012–9016.

38. Lu, Z., Yang, M., Chen, P., Xiong, X., and Li, A. (2014). Total synthesis of hapalindole-type natural products. Angew. Chem. Int. Ed. *53*, 13840–13844.

39. Meng, Z., Yu, H., Li, L., Tao, W., Chen, H., Wan, M., Yang, P., Edmonds, D. J., Zhong, J., and Li, A. (2015). Total synthesis and antiviral activity of indolosesquiterpenoids from the xiamycin and oridamycin families. Nat. Commun. *6*, 6096.

40. Zhou, S., Chen, H., Luo, Y., Zhang, W., and Li, A. (2015). Asymmetric total synthesis of mycoleptodiscin A. Angew. Chem. Int. Ed. *54*, 6878–6882.

41. Lu, Z., Li, H., Bian, M., and Li, A. (2015). Total synthesis of epoxyeujindole A. J. Am. Chem. Soc. *137*, 13764–13767.

42. Xiong, X., Zhang, D., Li, J., Sun, Y., Zhou, S., Yang, M., Shao, H., and Li, A. (2015). Synthesis of indole terpenoid mimics through a functionality-tolerated $Eu(fod)_3$-catalyzed conjugate addition. Chem. Asian J. *10*, 869–872.

43. Li, H., Chen, Q., Lu, Z., and Li, A. (2016). Total syntheses of aflavazole and 14-hydroxyaflavinine. J. Am. Chem. Soc. *138*, 15555–15558.

44. Pei, J., Zhou, S., Yang, F., Sun, Y., Li, A., Zhang, W.D., and He, W. (2016). Identification and mechanistic studies of a cell cycle regulator JP18 from a library of synthetic indole terpenoid mimics. Chem. Asian J. *11*, 2715–2718.

45. Kamenz, J. and Hauf, S. (2017). Time to split up: dynamics of chromosome separation. Trends Cell Biol. *27*, 42–54.

46. Nowak, S.J. and Corces, V.G. (2004). Phosphorylation of histone H3: a balancing act between chromosome condensation and transcriptional activation. Trends Genet. *20*, 214–220.

47. Warren, C.F.A., Wong-Brown, M.W., and Bowden, N.A. (2019). BCL-2 family isoforms in apoptosis and cancer. Cell Death Dis. *10*, 177.

48. Rogakou, E.P., Pilch, D.R., Orr, A.H., Ivanova, V.S., and Bonner, W.M. (1998). DNA double-stranded breaks induce histone H2AX phosphorylation on serine 139. J. Biol. Chem. *273*, 5858–5868.

49. Kaufmann, S.H., Desnoyers, S., Ottaviano, Y., Davidson, N.E., and Poirier, G.G. (1993). Specific proteolytic cleavage of poly(ADP-ribose) polymerase: an early marker of chemotherapy-induced apoptosis. Cancer Res. *53*, 3976–3985.

50. Lomenick, B., Hao, R., Jonai, N., Chin, R.M., Aghajan, M., Warburton, S., Wang, J., Wu, R.P., Gomez, F., Loo, J.A., Wohlschlegel, J.A., Vondriska, T.M., Pelletier, J., Herschman, H.R., Clardy, J., Clarke, C.F., and Huang, J. (2009). Target identification using drug affinity responsive target stability (DARTS). Proc. Natl. Acad. Sci. USA *106*, 21984–21989.

51. Pai, M.Y., Lomenick, B., Hwang, H., Schiestl, R., McBride, W., Loo, J.A., and Huang, J. (2015). Drug affinity responsive target stability (DARTS) for small-molecule target identification. Methods Mol. Biol. *1263*, 287–298.

52. Prota, A.E., Bargsten, K., Zurwerra, D., Field, J.J., Diaz, J.F., Altmann, K.H., and Steinmetz, M.O. (2013). Molecular mechanism of action of microtubule-stabilizing anticancer agents. Science *339*, 587–590.

53. Wallace, A.C., Laskowski, R.A., and Thornton, J.M. (1995). LIGPLOT: a program to generate schematic diagrams of protein-ligand interactions. Protein Eng. *8*, 127–134.

54. Lu, Y., Liu, Y., Xu, Z., Li, H., Liu, H., and Zhu, W. (2012). Halogen bonding for rational drug design and new drug discovery. Expert Opin. Drug Discov. *7*, 375–383.

55. Ravelli, R.B.G.; Gigant, B.; Curmi, P.A.; Jourdain, I.; Lachkar, S.; Sobel, A.; and Knossow, M. (2004). Insight into tubulin regulation from a complex with colchicine and a stathmin-like domain. Nature *428*, 198–202.

56. Wang, J., Miller D.D., and Li, W. (2022). Molecular interactions at the colchicine binding site in tubulin: an X-ray crystallography perspective. Drug Discov. Today *27*, 759–776.

57. van der Veen, A.G. and Ploegh, H.L. (2012). Ubiquitin-like proteins. Annu. Rev. Biochem. *81*, 323–357.

58. van Leuken, R., Clijsters, L., and Wolthuis, R. (2008). To cell cycle, swing the APC/C. Biochim. Biophys. Acta *1786*, 49–59.

59. Schrock, M.S., Stromberg, B.R., Scarberry, L., and Summers, M.K. (2020). APC/C ubiquitin ligase: Functions and mechanisms in tumorigenesis. Semin. Cancer Biol. *67*, 80–91.

60. Moreno-Moreno, O., Torras-Llort, M., and Azorin, F. (2019). The E3-ligases SCF^{Ppa} and APC/C^{Cdh1} co-operate to regulate CENP-A^{CID} expression across the cell cycle. Nucleic Acids Res. *47*, 3395–3406.

61. Mosca, L., Ilari, A., Fazi, F., Assaraf, Y.G., Colotti, G. (2021). Taxanes in cancer treatment: Activity, chemoresistance and its overcoming. Drug Resist. Updat. *54*, 100742.